

Electron–phonon decoupling due to strong light–matter interactions

Emil V. Denning,^{1,2} Matias Bundgaard-Nielsen,^{1,2} and Jesper Mørk^{1,2}

¹*Department of Photonics Engineering, Technical University of Denmark, DK-2800 Kgs. Lyngby, Denmark*

²*NanoPhoton - Center for Nanophotonics, Technical University of Denmark,*

Ørstedes Plads 345A, DK-2800 Kgs. Lyngby, Denmark

(Dated: June 5, 2022)

Phonon interactions in solid-state photonics systems cause intrinsic quantum decoherence and often present the limiting factor in emerging quantum technology. Due to recent developments in nanophotonics, exciton–cavity structures with very strong light–matter coupling rates can be fabricated. We show that in such structures, a new regime emerges, where the decoherence is completely suppressed due to decoupling of the dominant phonon process. Using a numerically exact tensor network approach, we perform calculations in this non-perturbative, non-Markovian dynamical regime. Here, we identify a strategy for reaching near-unity photon indistinguishability and also discover an interesting phonon-dressing of the exciton–cavity polaritons in the high- Q regime, leading to multiple phonon sidebands when the light–matter interaction is sufficiently strong.

The development of scalable solid-state quantum technology is challenged by lattice vibrations, i.e. phonons, which even at zero temperature deteriorates the quantum coherence [1, 2]. The interaction of electrons and phonons thus leads to remarkable features in the optical emission spectrum, such as broad spectral sidebands and incoherent scattering [3–7]. This is detrimental to the optical coherence and important to circumvent for applications in quantum technology. It also presents an open quantum system with rich physics, operating in a regime of pronounced non-Markovian dynamics [8].

Recent developments in nanophotonics have opened up the possibility of creating dielectric nanocavities with deep subwavelength confinement of light [9], leading to light–matter interaction strengths otherwise far beyond reach [10, 11]. Moreover, experiments have demonstrated very high coupling strengths between a plasmonic nanocavity and a pristine transition metal dichalcogenide monolayer [12–14]. These developments open the door to a new regime of nanophotonic electron–phonon interactions, where the light–matter coupling rate is comparable to or larger than the dominating phonon frequencies in the environment. In this paper, we study theoretically this new regime of cavity quantum electrodynamics and discover new and important effects. The comparability of phononic and optical time scales makes calculations of the dynamical properties highly challenging and has demanded extensive development of non-perturbative and non-Markovian theoretical methods [15–19]. To solve this outstanding problem, we have implemented a numerically exact and computationally efficient tensor network formulation [20, 21]. Furthermore, we make use of a variational polaron perturbation theory to derive analytical results that explain the dynamical decoupling process. As an example, we consider a nanocavity containing a semiconductor quantum dot, which is coupled to the longitudinal acoustic phonon modes of the host lattice. With this example, we show that the spectral phonon sideband can be completely suppressed, when the

nanocavity is in the low- Q Purcell regime and the light–matter interaction strength exceeds the phonon cutoff frequency. Additionally, we predict a novel effect in the high- Q limit, where each of the exciton polariton peaks in the spectrum is dressed with an individual phonon sideband, demonstrating non-perturbative dynamics, where polaritons and polarons occur at an equal footing.

Our analysis is based on a generic system consisting of a localised exciton state, $|X\rangle$, a cavity mode with annihilation operator a and a vibrational environment with phonon annihilation operators $\{b_{\mathbf{k}}\}$. The exciton–phonon coupling is described by the Hamiltonian [22]

$$H_{ep} = |X\rangle\langle X| \sum_{\mathbf{k}} \hbar(g_{\mathbf{k}}b_{\mathbf{k}} + g_{\mathbf{k}}^*b_{\mathbf{k}}^\dagger), \quad (1)$$

where $\{g_{\mathbf{k}}\}$ are the exciton–phonon coupling strengths. The influence of the vibrational environment is characterised by the spectral density, $J(\nu) = \sum_{\mathbf{k}} |g_{\mathbf{k}}|^2 \delta(\nu - \nu_{\mathbf{k}})$, where $\nu_{\mathbf{k}}$ is the frequency of the phonon mode with momentum \mathbf{k} . For any realistic physical system, this spectral density has a cutoff frequency, ξ , such that $J(\nu) \simeq 0$ for $\nu \gg \xi$. This cutoff frequency is related to the length scale of the exciton wavefunction and the properties of available phonon modes in the material [22–24]. The light–matter interaction is governed by the Hamiltonian $H_0 = \hbar\delta a^\dagger a + \hbar g(|0\rangle\langle X| a^\dagger + |X\rangle\langle 0| a)$, where $\delta = \omega_c - \omega_X$ is the cavity–exciton detuning, g is the light–matter coupling strength and $|0\rangle$ is the electronic ground state. Furthermore, cavity losses with a rate κ and exciton dephasing with a temperature-dependent rate $\gamma^*(T)$ are treated through the Lindblad formalism [25, 26] as Markovian effects [27–29]. To describe the optical emission properties of the system, we initialise it in the exciton state with zero photons in the cavity and calculate the spectral correlation function of the emitted photons as the system relaxes, $S(\omega, \omega') = \kappa \langle a^\dagger(\omega) a(\omega') \rangle = \kappa \int_{-\infty}^{\infty} dt \int_{-\infty}^{\infty} dt' e^{-i(\omega t - \omega' t')} \langle a^\dagger(t') a(t) \rangle$. From this spectral function, we can calculate the emission spectrum as $S(\omega, \omega)$ [30]. In addition, it provides ac-

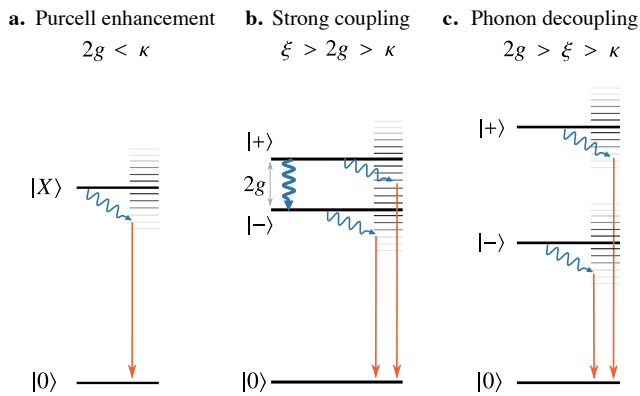


FIG. 1. Illustration of phonon-mediated optical emission processes. **a.** In the Purcell regime, the exciton decays and emits a photon (orange arrow). During this process, a phonon wavepacket (blue wiggly arrow) might be emitted or absorbed, resulting in a photon with lower or higher energy. **b.** In the strong light–matter coupling regime, a phonon wavepacket can be emitted either by relaxation from the upper polariton to the lower one (downwards wiggly arrow), or when one of the polaritons decays to the ground state. **c.** In the phonon decoupling regime, where the polariton splitting, $2g$, exceeds the phonon cutoff frequency, ξ , the phonon sidebands on the two polaritons do not overlap and are hence spectrally resolved.

cess to the coherence properties of the emitted photons, for example their indistinguishability [31], $\mathcal{I} = [\int d\omega S(\omega, \omega)]^{-2} \int d\omega \int d\omega' |S(\omega, \omega')|^2$, which quantifies the interference visibility of two subsequently emitted photons.

There are three main parameter regimes of this system: In the Purcell regime (Fig. 1a), where $2g < \kappa$, the exciton decays and emits a photon into the cavity with a rate of $\Gamma_p = 4g^2/\kappa$. In this process, a phonon wavepacket may be emitted or absorbed, generating a broad sideband in the emission spectrum. At low temperatures, $k_B T \ll \hbar\xi$, the sideband is asymmetric and red-detuned from the zero-phonon line, reflecting that phonon emission dominates over phonon absorption [32]. In the strong coupling regime (Fig. 1b), the coupling strength exceeds the decay, $2g > \kappa$, but is still well below the phonon cutoff frequency. Here, the exciton and cavity form hybrid polaritons, $|\pm\rangle = |1, 0\rangle \pm |0, X\rangle$ (where $|n, e\rangle$ denotes a n -photon cavity state and electronic state $e \in \{0, X\}$) that are spectrally well-resolved and split by a frequency of $2g$. The dominating decoherence mechanism in this regime arises from a resonant transition from the upper polariton to the lower polariton under the emission of a phonon wavepacket with energy $\sim 2\hbar g$. If the temperature is sufficiently high to populate the phonon modes, the reverse process can also take place by phonon absorption. At low temperatures, the phonon emission process, $|+\rangle \rightarrow |-\rangle$, dominates, and a spectral polariton asymmetry can be observed, because photons are thus predominantly emit-

ted from the lower polariton state [16, 33, 34]. Since the polariton splitting is small compared to the phonon cutoff frequency, the sideband seen in the Purcell regime is not resolved into contributions from the two polaritons.

Increasing the coupling strength further leads to a regime of phonon decoupling (Fig. 1c), where $2g$ exceeds the phonon cutoff frequency. Due to this, there are no phonon modes with sufficiently high energy to drive polariton transitions, and this decoupling leads to a recovery of the quantum coherence. Additionally, the spectral symmetry between the polariton peaks is restored and the polaritons are now so far separated that the individual phonon-polariton sidebands are spectrally resolved.

Calculating the temporal correlation function entering $S(\omega, \omega')$ is a technically demanding task due to the non-Markovian interactions with the phonon environment. Our approach, based on a tensor-network representation of the phonon influence functional, is described in the Supplementary Material. To illustrate the three different regimes in Fig. 1, we use a semiconductor quantum dot in a nanocavity as an example. Here, the phonon cutoff frequency is typically on the order of a few ps^{-1} [34], and the spectral density is $J(\nu) = \alpha\nu^3 \exp\{-(\nu/\xi)^2\}$, where α is an overall phonon coupling strength [24]. The optical emission spectra for parameters corresponding to the three characteristic parameter regimes are shown in Fig. 2. The spectra in the upper panels are calculated for a temperature of $T = 4$ K, and in the lower panels for $T = 150$ K.

In the Purcell regime (Fig. 2a-b), the spectrum exhibits a narrow zero-phonon line dressed by a broad phonon sideband, which is asymmetric in the low-temperature limit. In addition, thermal phonon scattering and dephasing broadens the zero-phonon line at higher temperatures. In the strong coupling regime (Fig. 2c-d), the polariton peaks are asymmetric at low temperature, and the polariton peaks are dressed by a single phonon sideband. In the regime of phonon decoupling (Fig. 2e-f), the polaritons are split beyond the phonon cutoff frequency, and thus the polaritons are dressed by spectrally resolved sidebands. Furthermore, the polariton symmetry in the spectrum is recovered.

To understand the complex behaviour of the system, we apply a variational polaron transformation to the Hamiltonian. This transformation is generated by the operator $V = |X\rangle\langle X| \sum_{\mathbf{k}} f_{\mathbf{k}} (b_{\mathbf{k}}^\dagger - b_{\mathbf{k}}) / \nu_{\mathbf{k}}$ and transforms the Hamiltonian as $H_V = e^V H e^{-V}$. Here, $f_{\mathbf{k}}$ are variational coefficients, which are determined such that the Feynman-Bogoliubov bound on the free energy is minimized [24, 35, 36]. In practise, this means that the transformation depends on the relative magnitude of g and ξ . An important characteristic of the transformation is the variational renormalisation factor, $B_V = \langle e^{\pm V} \rangle$, which depends on g and takes a value between 0 and 1, such that $B_V \simeq 1$ when $2g \gg \xi$ (see Fig. 3a). The significance of B_V is two-fold: First, the light–matter interac-

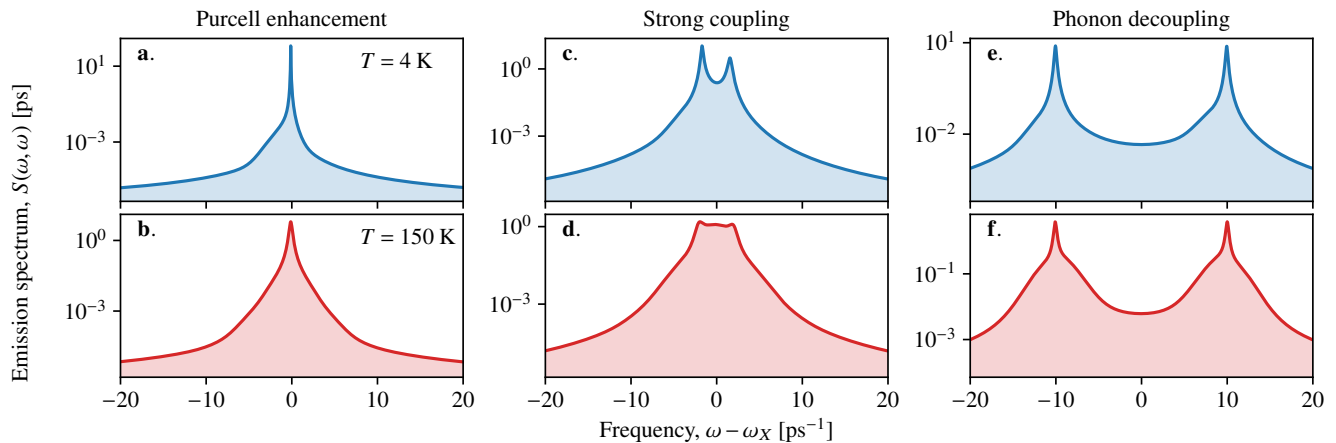


FIG. 2. Optical emission spectra in the **a.-b.** Purcell regime $g = 0.05 \text{ ps}^{-1}$, $\kappa = 0.5 \text{ ps}^{-1}$, **c.-d.** strong coupling regime, $g = 1.1 \text{ ps}^{-1}$, $\kappa = 0.5 \text{ ps}^{-1}$, and **e.-f.** phonon decoupling regime, $g = 10.0 \text{ ps}^{-1}$, $\kappa = 0.5 \text{ ps}^{-1}$. For the upper panels, the temperature is $T = 4 \text{ K}$, and for the lower panels, $T = 150 \text{ K}$. We have used an overall phonon coupling strength, $\alpha = 0.025 \text{ ps}^2$ and phonon cutoff frequency, $\xi = 2.23 \text{ ps}^{-1}$. The cavity and exciton were taken resonant, $\omega_c = \omega_X + R_v$.

tion in the transformed Hamiltonian, H_v , is renormalised as $g \rightarrow gB_v$, meaning that the phonons reduce the effective coupling strength. Furthermore, when the exciton-cavity system is in the Purcell regime, $2g < \kappa$, and $\kappa > \xi$, the probability of generating a phonon wavepacket jointly with the emission of a photon is given by $1 - B_v^2$, i.e. the phonon sideband constitutes a fraction of $1 - B_v^2$ of the total emission spectrum; in the limit $g \rightarrow 0$, B_v^2 reduces to the Franck-Condon factor [2]. However, as shown in Fig. 2c-d, this branching ratio does not hold in the phonon decoupling regime, where the polariton peaks are dressed with a phonon sideband, even though g is sufficiently large to ensure $B_v \simeq 1$. Thus, the polaritonic phonon sidebands are a strongly non-perturbative effect that cannot be captured even by the optimal perturbation theory. In analogy with the coupling strength renormalisation, the variational transformation also shifts the exciton resonance by $R_v = \sum_{\mathbf{k}} f_{\mathbf{k}}(f_{\mathbf{k}} - 2g_{\mathbf{k}})/\nu_{\mathbf{k}}$. This effect is of minor importance, but needs to be taken into account when setting the cavity frequency to resonance with the exciton.

To investigate the overall influence of the phonons in the decoupling regime, the photon indistinguishability is shown in Fig. 3b as a function of g . The blue line with open circles signify a configuration with fixed cavity decay rate, corresponding to the blue spectra in the upper panels of Fig. 2. Here, it is clearly seen that the impact of the phonon environment is most significant when $J(2g)$ is maximal, meaning that the scattering process from the upper polariton to the lower is resonantly enhanced, and the photon emission process is exposed to strong decoherence. However, when $2g$ exceeds the cutoff frequency, the indistinguishability converges to ~ 0.95 , due to the persistent polariton phonon sidebands. Alternatively, the orange line with dots shows the indistinguishability in a

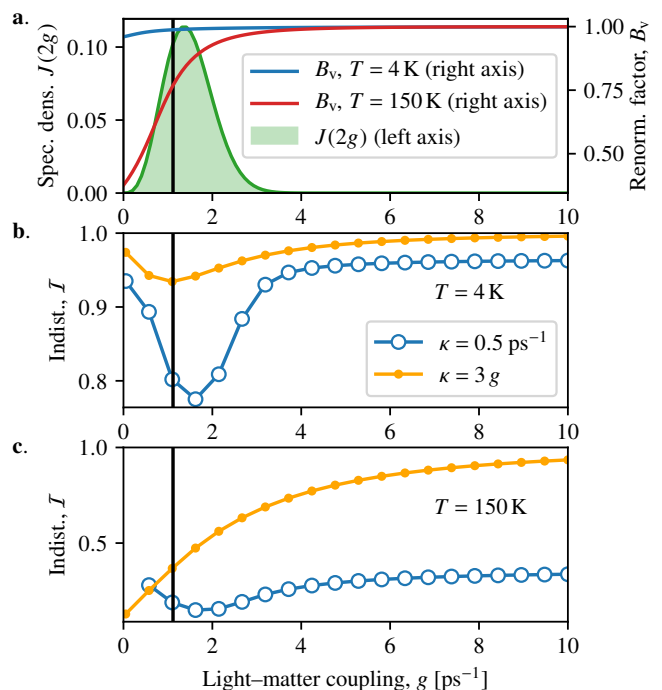


FIG. 3. **a.** Phonon spectral density evaluated at $\nu = 2g$ (green, left axis) and variational renormalisation factor, B_v , (right axis) at $T = 4 \text{ K}$ (blue) and $T = 150 \text{ K}$ (red) as a function of the light-matter coupling strength, g . The phonon cutoff frequency is indicated as $\xi/2$ by a solid black line. **b.** Photon indistinguishability as a function of light-matter coupling strength, g for fixed cavity decay, $\kappa = 0.5 \text{ ps}^{-1}$ (blue line and open circles) and cavity decay rate pinned to the coupling strength, $\kappa = 3g$ (orange line and dots) at $T = 4 \text{ K}$. **c.** Same as in b., but at $T = 150 \text{ K}$. The line signatures are the same as in panel b.

Purcell-configuration, where κ is pinned at $3g$, ensuring that the system never enters the strong coupling regime. Here, the phonon sideband can be completely eliminated, when $B_v \rightarrow 1$ and the zero-phonon line broadens sufficiently to absorb the entire sideband.

The difference between the polariton and Purcell regimes becomes even more pronounced in the high-temperature limit (Fig. 3c), where the sideband is more dominating in the spectrum. Due to thermal phonon population, the exciton dephasing here is stronger, meaning that the increase in indistinguishability for the Purcell configuration is slower than for the low-temperature case. It is noteworthy that even at this high temperature, it is possible to achieve phonon decoupling and thus near-unity indistinguishability.

We now turn our attention towards the phonon-induced polariton asymmetry in the spectrum that arises when the upper polariton decays to the lower polariton, which is the dominant dephasing mechanism in the strong coupling regime at low temperatures. In Fig. 4, we show, as a function of g , the spectral asymmetry between the polariton peaks (solid line and open circles, left axis), calculated as $A = (S_- - S_+) / (S_- + S_+)$, where $S_{\pm} := S(\omega_{\pm}, \omega_{\pm})$ is the emission spectrum evaluated at the upper (+) and lower (-) polariton peak. As expected, the polariton symmetry is recovered in the limit $2g \gg \xi$. To support this finding, we use a master equation in the variational frame to derive the asymmetry-driving differential scattering rate from the upper to the lower polariton (see Supplementary Material),

$$\Gamma_A = \frac{\pi}{2} J(2gB_v)[1 - F^2(2gB_v)] + \epsilon(g), \quad (2)$$

where $F(\nu)$ is the dimensionless variational displacement function, $F(\nu_{\mathbf{k}}) = f_{\mathbf{k}}/g_{\mathbf{k}}$ and $\epsilon(g)$ is a small term that vanishes in the limit $2g \gg \xi$. This analytical scattering rate is also shown in Fig. 4 (shaded area, right axis) and exhibits a similar behaviour as the polariton asymmetry. These findings show that the phonon-induced polariton scattering can indeed be eliminated in the phonon decoupling regime, because there are no available phonon modes with sufficiently high frequency to match the polariton energy difference. However, as shown in Figs. 2 and 3, this does not mean that the phonons are fully decoupled in this regime, since the polaritonic phonon sidebands do not rely on resonant transitions, but occur due to vibrational dressing of the individual polaritons.

In conclusion, we have shown that the phonons in the environment of a localised exciton coupled to a nanocavity can be dynamically decoupled when the light-matter coupling is sufficiently strong. We have found that an effective decoupling occurs in the Purcell regime, where the zero-phonon transition occurs with a rate much higher than the phonon cutoff frequency. Furthermore, we have found that the phonon-induced polariton scattering in the strong light-matter coupling regime can be elimi-

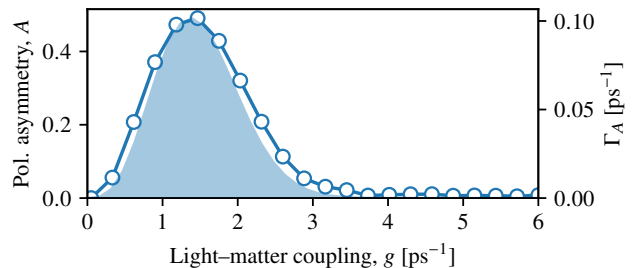


FIG. 4. Asymmetry of polariton peaks, A , as a function of coupling strength (solid line and open circles, left axis), overlaid with analytically calculated differential polariton scattering rate, Γ_A (shaded area, right axis).

nated when the polariton splitting exceeds the phonon cutoff frequency. However, we also find a significant phonon-dressing of the individual polaritons that persists into the phonon decoupling regime, demonstrating the importance of operating in the Purcell regime. These principal observations only rely on the relative magnitude of the exciton-cavity coupling strength and the phonon cutoff frequency, and generally hold for any exciton-cavity system.

Acknowledgements — The authors thank Mathias R. Jørgensen for helpful discussions. This work was supported by the Danish National Research Foundation through NanoPhoton - Center for Nanophotonics, grant number DNRF147.

-
- [1] K.-M. C. Fu, C. Santori, P. E. Barclay, L. J. Rogers, N. B. Manson, and R. G. Beausoleil, *Physical Review Letters* **103**, 256404 (2009).
 - [2] J. Iles-Smith, D. P. S. McCutcheon, A. Nazir, and J. Mørk, *Nature Photonics* **11**, 521 (2017).
 - [3] A. J. Brash, J. Iles-Smith, C. L. Phillips, D. P. S. McCutcheon, J. O'Hara, E. Clarke, B. Royall, L. R. Wilson, J. Mørk, M. S. Skolnick, *et al.*, *Phys. Rev. Lett.* **123**, 167403 (2019).
 - [4] T. T. Tran, C. Zachreson, A. M. Berhane, K. Bray, R. G. Sandstrom, L. H. Li, T. Taniguchi, K. Watanabe, I. Aharonovich, and M. Toth, *Physical Review Applied* **5**, 034005 (2016).
 - [5] D. Christiansen, M. Selig, G. Berghäuser, R. Schmidt, I. Niehues, R. Schneider, A. Arora, S. M. de Vasconcellos, R. Bratschitsch, E. Malic, *et al.*, *Physical Review Letters* **119**, 187402 (2017).
 - [6] M. W. Doherty, N. B. Manson, P. Delaney, F. Jelezko, J. Wrachtrup, and L. C. L. Hollenberg, *Physics Reports* **528**, 1 (2013).
 - [7] M. Selig, G. Berghäuser, A. Raja, P. Nagler, C. Schüller, T. F. Heinz, T. Korn, A. Chernikov, E. Malic, and A. Knorr, *Nature Communications* **7**, 1 (2016).
 - [8] A. Carmele and S. Reitzenstein, *Nanophotonics* **8**, 655 (2019).

- [9] H. Choi, M. Heuck, and D. Englund, *Physical Review Letters* **118**, 223605 (2017).
- [10] S. Hu, M. Khater, R. Salas-Montiel, E. Kratschmer, S. Engelmann, W. M. Green, and S. M. Weiss, *Science Advances* **4**, eaat2355 (2018).
- [11] F. Wang, R. E. Christiansen, *et al.*, *Applied Physics Letters* **113**, 241101 (2018).
- [12] J. Qin, Y.-H. Chen, Z. Zhang, Y. Zhang, R. J. Blaikie, B. Ding, and M. Qiu, *Physical Review Letters* **124**, 063902 (2020).
- [13] M. Geisler, X. Cui, J. Wang, T. Rindzevicius, L. Gammelgaard, B. S. Jessen, P. A. D. Goncalves, F. Todisco, P. Bøggild, A. Boisen, M. Wubs, N. A. Mortensen, S. Xiao, and N. Stenger, *ACS Photonics* **6**, 994 (2019).
- [14] M.-E. Kleemann, R. Chikkaraddy, E. M. Alexeev, D. Kos, C. Carnegie, W. Deacon, A. C. De Pury, C. Große, B. De Nijs, J. Mertens, *et al.*, *Nature Communications* **8**, 1 (2017).
- [15] A. Morreau, C. Joshi, and E. A. Muljarov, arXiv preprint arXiv:2002.01912 (2020).
- [16] A. Morreau and E. Muljarov, *Physical Review B* **100**, 115309 (2019).
- [17] A. Vagov, M. D. Croitoru, M. Glässl, V. M. Axt, and T. Kuhn, *Physical Review B* **83**, 094303 (2011).
- [18] P. Kaer, T. R. Nielsen, P. Lodahl, A.-P. Jauho, and J. Mørk, *Physical Review Letters* **104**, 157401 (2010).
- [19] P. Kaer, P. Lodahl, A.-P. Jauho, and J. Mørk, *Physical Review B* **87**, 081308 (2013).
- [20] M. R. Jørgensen and F. A. Pollock, *Physical Review Letters* **123**, 240602 (2019).
- [21] A. Strathearn, P. Kirton, D. Kilda, J. Keeling, and B. W. Lovett, *Nature Communications* **9**, 1 (2018).
- [22] G. D. Mahan, *Many-particle physics* (Springer Science & Business Media, 2013).
- [23] A. Alkauskas, B. B. Buckley, D. D. Awschalom, and C. G. Van de Walle, *New Journal of Physics* **16**, 073026 (2014).
- [24] A. Nazir and D. P. S. McCutcheon, *Journal of Physics: Condensed Matter* **28**, 103002 (2016).
- [25] H.-P. Breuer and F. Petruccione, *The theory of open quantum systems* (Oxford University Press on Demand, 2002).
- [26] G. Lindblad, *Communications in Mathematical Physics* **48**, 119 (1976).
- [27] A. Reigue, J. Iles-Smith, F. Lux, L. Monniello, M. Bernard, F. Margailan, A. Lemaitre, A. Martinez, D. P. S. Mccutcheon, J. Mørk, *et al.*, *Physical Review Letters* **118**, 233602 (2017).
- [28] P. Tighineanu, C. L. Dreessen, C. Flindt, P. Lodahl, and A. S. Sørensen, *Physical Review Letters* **120**, 257401 (2018).
- [29] E. A. Muljarov and R. Zimmermann, *Physical Review Letters* **93**, 237401 (2004).
- [30] D. A. Steck, “Quantum and atom optics,” (2007).
- [31] A. Kiraz, M. Atatüre, and A. Imamoglu, *Physical Review A* **69**, 032305 (2004).
- [32] B. Krummheuer, V. M. Axt, and T. Kuhn, *Physical Review B* **65**, 195313 (2002).
- [33] K. Roy-Choudhury and S. Hughes, *Physical Review B* **92**, 205406 (2015).
- [34] E. V. Denning, J. Iles-Smith, N. Gregersen, and J. Mørk, *Optical Materials Express* **10**, 222 (2020).
- [35] D. P. S. McCutcheon, N. S. Dattani, E. M. Gauger, B. W. Lovett, and A. Nazir, *Physical Review B* **84**, 081305 (2011).
- [36] O. J. Gómez-Sánchez and H. Y. Ramírez, *Physical Review A* **98**, 053846 (2018).